
ORTHOGONAL VORONOI DIAGRAM AND TREEMAP

A PREPRINT

Yan-Chao Wang

School of Computer Science and Engineering
Nanyang Technological University
Singapore
ywang054@e.ntu.edu.sg

Feng Lin

School of Computer Science and Engineering
Nanyang Technological University
Singapore
asflin@ntu.edu.sg

Hock-Soon Seah

School of Computer Science and Engineering
Nanyang Technological University
Singapore
ashsseah@ntu.edu.sg

April 5, 2019

ABSTRACT

In this paper, we propose a novel space partitioning strategy for implicit hierarchy visualization such that the new plot not only has a tidy layout similar to the treemap, but also is flexible to data changes similar to the Voronoi treemap. To achieve this, we define a new distance function and neighborhood relationship between sites so that space will be divided by axis-aligned segments. Then a sweepline+skyline based heuristic algorithm is proposed to allocate the partitioned spaces to form an orthogonal Voronoi diagram with orthogonal rectangles. To the best of our knowledge, it is the first time to use a sweepline-based strategy for the Voronoi treemap. Moreover, we design a novel strategy to initialize the diagram status and modify the status update procedure so that the generation of our plot is more effective and efficient. We show that the proposed algorithm has an $O(n \cdot \log(n))$ complexity which is the same as the state-of-the-art Voronoi treemap. To this end, we show via experiments on the artificial dataset and real-world dataset the performance of our algorithm in terms of computation time, converge rate, and aspect ratio. Finally, we discuss the pros and cons of our method and make a conclusion.

Keywords Orthogonal rectangle · Voronoi diagram · Voronoi treemap · hierarchy visualization · treemap · axis-aligned rectangle

1 Introduction

Hierarchical data visualization plays an essential role in the field of information visualization since hierarchical data structures are quite common in our daily life, including file systems, software/package class structures, and the organization structure of companies. Thus, a large number of hierarchy visualization methods have been developed to depict the dataset from different aspects [1, 2]. Some of them explicitly show the hierarchical structure as straight lines, arcs, or curves, while others focus on the value within each node and positionally encode the hierarchy by node overlap or inclusion. Hence, these methods implicitly presenting the hierarchy are considered more space efficient [3]. Treemap [4] and Voronoi treemap [5] which are formed by nested rectangles and polygons respectively are the most two popular implicit hierarchy visualization methods. However, they adopt distinct strategies to generate the plots. Treemap method divides the empty canvas into rectangular sub-regions so that the area is associated with the relative sizes of the respective sub-hierarchies. Meanwhile, Voronoi treemap partitions the canvas into polygon shapes based on distance to beforehand specified sites. After that, the position and weight of the sites may be iteratively adapted in order to adjust the area of the sub-regions.

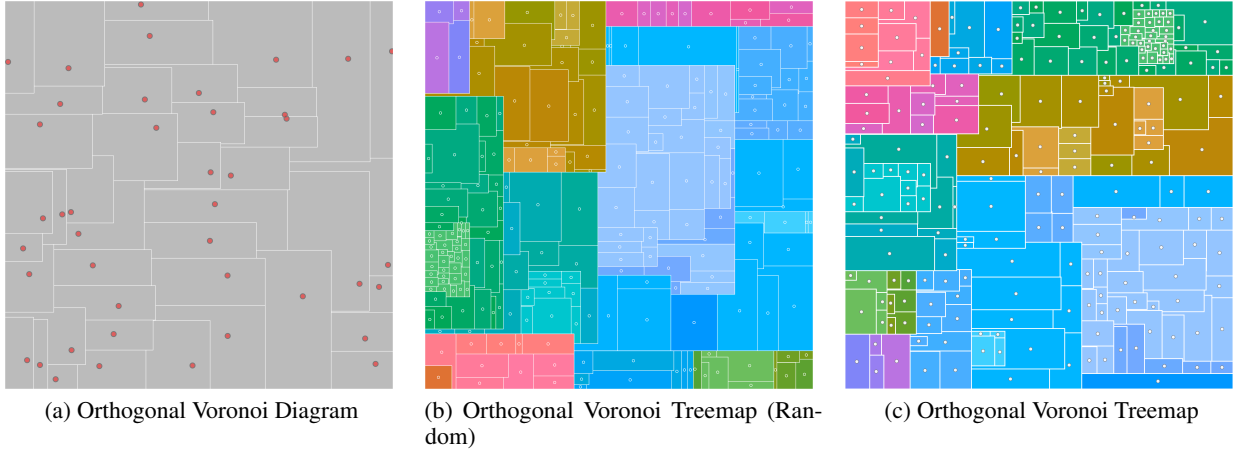


Figure 1: Orthogonal Voronoi diagram and orthogonal Voronoi treemap. (a) The orthogonal Voronoi diagram is generated based on the positions of a series of random points. (b) The orthogonal Voronoi treemap visualizes the Flare class hierarchy (colored by TreeColors [12]) with random initial status. (c) The orthogonal Voronoi treemap uses the squarified treemap as initial status.

In our opinion, the treemap and the Voronoi treemap make different choices in terms of shape simplicity and adjustment ability. To be specific, by using rectangular shapes, the treemap is more comfortable and much tidier for the viewers than Voronoi treemap with nested polygons. Moreover, rectangle shapes make it easier to visually compare the areas of different regions than polygon shapes [6]. However, when the hierarchical data changes even slightly, the partitioning of empty canvas in treemap need to be regenerated and the new layout may be largely different from the previous one. It usually leads to bad layout stability. In contrast, Voronoi treemap can adjust its layout via slight modification on the status of its sites.

We aim to find a good balance between shape simplicity and adjustment ability with the proposed novel hierarchy visualization method: orthogonal Voronoi diagram and treemap. The orthogonal layout has been proved to suitable for human beings in explicit hierarchy visualization (node-link diagram) and network visualization [7, 8]. It would be an interesting topic to evaluate different treemap layouts in implicit hierarchy visualization. A treemap with orthoconvex and L-shape was proposed by dividing existing treemap element to preserve an aspect ratio constraint [9]. However, the orthoconvex treemap cannot be adjusted flexibly.

Our orthogonal Voronoi diagram partitions the empty canvas into nested orthogonal rectangles. Hence, the generated layout is not only flexible to a diversified data value, but also much tidier than the Voronoi treemap with nested polygons. To achieve this, we first define a new distance calculation strategy in order to generate axis-aligned segmentation among the sites. In the strategy, a new distance function is defined by considering the relative positions of two sites rather than a single site. Then a horizontal or vertical segmentation line is generated between these two sites. After that, we design a sweepline + skyline heuristic algorithm to partition the canvas based on the new distance calculation strategy to generate an orthogonal Voronoi diagram. The proposed algorithm is motivated by the sweep line algorithm for Voronoi diagram generation [10] and the skyline strategy in handling cutting and packing problems [11]. By iteratively alerting the status of the original sites and calling the sweepline + skyline algorithm, the area of the orthogonal rectangular sub-regions will match their corresponding values. An orthogonal Voronoi treemap will be obtained if this process is recursively continued layer by layer until the whole hierarchical structure is traversed. Moreover, we also design an initialization strategy to improve algorithm performance. The proposed algorithm is fast, simple, and resolution-independent. Figure 1 gives examples of the proposed orthogonal Voronoi diagram (on a series of random sites marked in red with zero weight) and the orthogonal Voronoi treemap (of the hierarchical structure of the Flare classes, starting from different initial statuses).

The main contribution of this paper is threefold: First, we define a novel distance function based on two sites so that the segmentation is axis-aligned. Second, we design a sweepline + skyline algorithm for space partitioning with $O(n \cdot \log(n))$ complexity. To the best of our knowledge, this is the first time the sweep line strategy is used for the Voronoi treemap. Third, we design a novel strategy to initialize the diagram status and modify the status update procedure to increase the efficiency and effectiveness of our algorithm.

The rest of this paper is organized as follows. The related work about our orthogonal Voronoi treemap is reviewed in Sect. 2. The background knowledge is introduced in Sect. 3 before the description of our methodology. In Sect. 4, we describe the proposed orthogonal space partitioning algorithm to generate the orthogonal Voronoi treemap. The performance of our algorithm is depicted in Sect. 5. Finally, discussion and conclusion are made in Sect. 6 and Sect. 7.

2 Related Work

In this section, we give an overview of implicit hierarchy visualization methods which are related to our work. We mainly focus on the canvas subdivision strategies used to generate layouts, instead of including all implicit visualization techniques. Based on whether the sites are referred to during the subdivision, we divide the methods into two clusters: non-site-based methods and site-based methods. Both of them belong to methods with inclusion edge representation according to the design space definition [3].

Non-site-based Methods Implicit hierarchy visualization methods that partition the whole space without considering the sites are treated as non-site-based methods, such as the treemap. These methods position the data by following some rules or experience in order to get expected configurations, which sometimes are also named as heuristic-based algorithm. Starting from the propose of original treemap in 1992 [4], a large number of variants are proposed in the literature [1, 13].

The squarified treemap focuses on the emergence of thin, elongated rectangles in the standard treemaps and presents a new subdivision method such that the resulting rectangles have a lower aspect ratio [14]. The ordered treemap layout is the first type of treemap layout that takes stability into consideration [15]. In their work, two pivot based algorithms (pivot-by-size and pivot-by-middle) are proposed to ensure that items near each other in the original data will be near each other in the final layout. The split algorithm used in the ordered and quantum treemaps [16] is a modification of the squarified treemaps, following a given one-dimensional ordering. The spiral treemap positions the one-dimensional ordering of the input data along the border following a circular arrangement or an S-shape [17]. Different from previous methods which only consider one dimension, the spatially order treemaps consider two-dimensional consistency by relating node order to Euclidean distance from the parent node’s top-left corner [18]. We observe that the layout generation problem in treemap is quite similar to the two-dimensional (2D) bin packing which is an optimization problem with a wide range of applications in resource management. This observation was also mentioned by Schulz et al. [3]. Since many heuristic algorithms [11, 19] have been proposed to solve the bin packing problem, how to utilize them into the layout generation in treemap would be an interesting research direction and we find that some researchers have started to do this [20, 21].

Non-rectangular treemaps are also designed in the literature. Jigsaw map has nicely shaped regions and stable layout by considering Hilbert curves or H curves [22]. They generate irregular shapes which are not easy to be compared with. A modification then was proposed by splitting the space into rectangles [23]. To relax rectangular constraint, angular treemaps describe a divide-and-conquer method to partition the space into various shapes [24]. Besides that, the treemap layout that produces irregular nested shapes by subdividing the Gosper curve [25] was also proposed.

Site-based Methods Some implicit hierarchy visualization methods partition the space based on a series of pre-defined sites, such as the Voronoi treemap. The Voronoi treemap was originally presented by Balzer et al. [5]. By relaxing the constraint of rectangular shapes, they utilize Voronoi tessellations to generate polygonal subdivisions. They firstly initialize a set of sites with initial weight values and then compute the Voronoi tessellations based on distance functions. By adaptively altering the weight value of each site, it enables a dedicated Voronoi region in the next iteration step. Finally, the computation will be stopped when a good enough layout is reached. Later, the Voronoi treemaps are utilized to visualize dynamic hierarchical data owing to its adjustment ability [26, 27]. However, the calculation of these Voronoi treemaps is computationally expensive as a random-sampling strategy is used to compute the Voronoi tessellations. In 2012, Nocaj and Brandes [28] proposed a resolution-independent algorithm by calculating the Voronoi tessellations with power diagrams, such that the new algorithm is faster in both theory and practice. An improvement is then made by setting an initial position for visualizing varying hierarchies [29].

Neighborhood treemap (Nmap) [6], that successively bisects a set of pre-defined sites on the horizontal or vertical directions and then scales the bisections to match the value of each site, is also a site-based method. Although no distance function is used during the segmentation, Nmap also needs sites representing the similarity relationships of data elements to be positioned in the canvas. Thus, Nmap can preserve similarity relationship among data elements very well. However, no evidence shows that Nmap can produce stable layouts with dynamic data. Circle packing [30] can also be treated as a site-based method since the generation of the layouts is based on the center of each circle, as well as the recently proposed bubble treemaps [31].

3 Background

In this section, we review the background on the Voronoi treemap, including Voronoi diagram, weighted Voronoi diagram, centroidal Voronoi diagram, and Voronoi treemap. In the description, we follow the notation used in Nocaj and Brandes's work [28].

3.1 Voronoi Diagram

A Voronoi diagram (also called a Voronoi tessellation, or a Voronoi partition) is a partitioning of a plane into sub-regions based on distances to a set of points within the plane. These sub-regions are often called *Voronoi cell* (or *cell*) and these points in the plane are called *sites*. In this paper, we only consider the partitioning in a bounded region (e.g. a rectangle) rather than the whole 2D plane.

Formally, given a bounded region $\Omega \subset R^2$ and a set of n sites $S = \{s_1, s_2, \dots, s_n\}$, the Voronoi diagram divides Ω into a set of Voronoi cells $v(s_i)$, one for each site s_i . Then the cell $v(s_i)$ can be expressed as

$$v(s_i) = \{p \in \Omega \mid \text{dist}(p, s_i) < \text{dist}(p, s), \forall s \in S, s \neq s_i\}, \quad (1)$$

where $\text{dist}(p, s_i)$ is the distance between point $p = (x_p, y_p)$ and site $s_i = (x_{s_i}, y_{s_i})$. The distance can be the Euclidean distance or other distance functions. The most two often used distance functions are the Euclidean distance $\text{dist}_e(p, s_i)$ and the power Euclidean distance $\text{dist}_{pe}(p, s_i)$ which are shown as below:

$$\text{dist}_e(p, s_i) = \|p - s_i\| = \sqrt{(x_p - x_{s_i})^2 + (y_p - y_{s_i})^2}, \quad (2)$$

$$\text{dist}_{pe}(p, s_i) = \|p - s_i\|^2 = (x_p - x_{s_i})^2 + (y_p - y_{s_i})^2. \quad (3)$$

Thus, the Voronoi diagram is defined as the collection of Voronoi cells, $v(S) = \{v(s_1), \dots, v(s_n)\}$.

3.2 Weighted Voronoi Diagram

In the Voronoi diagram, the area of a cell is fixed and only depends on the positions of its associated and neighboring sites. Hence, in order to use the cells to depict additional information (e.g. data value), a mechanism to control the areas of cells is required. To achieve this, a positive real weight is associated with each site. When calculating the distance, the associated weights should also be taken into account.

Since the power Euclidean distance function produces a straight line between two sites (the solid black lines in Fig. 3), thus in this paper the Voronoi plots are all based on the power Euclidean distance with the exception of our proposed orthogonal Voronoi plots that is based on a new distance function.

Formally, let $W = \{w_1, w_2, \dots, w_n\}$ be a set of positive weights associated with the set of sites S correspondingly. Then the weighted power Euclidean distance based on the original power Euclidean distance (Eq. 3) can be written as follows:

$$\text{dist}_{awpe}(p, s_i) = \|p - s_i\|^2 - w_i. \quad (4)$$

Increasing the weight value will increase the area of the cell. However, it is nonlinear in general. Besides that, a too large weight value may lead to empty cells. We will discuss this overweight issue in the description of our algorithms.

3.3 Centroidal Voronoi Diagram

Centroidal Voronoi diagram is a special type of Voronoi diagram that the site s_i is located at the center of each cell $v(s_i)$ [32]. This kind of diagram usually can generate cells with good aspect ratio (i.e. the ratio of the sides of the oriented minimum bounding rectangle is close to one). This is relevant because a good aspect ratio ensures a good readability in visualization. Let $\overline{v(s_i)}$ and $A(\overline{v(s_i)})$ be the polygonal boundary and area of cell $v(s_i)$ respectively, the centroid $c_i = \text{centroid}(\overline{v(s_i)})$ can be calculated in linear time. For all the n sites, the computation of the centroid needs $O(n)$ time.

3.4 Voronoi Treemap

The Voronoi treemap is a recursive partitioning of a plane, the same as the treemap. Starting from the root of a hierarchy, a weighted Voronoi diagram is generated in the region Ω with one cell for each child of the root. An iterative optimization process is taken to adaptively alert the value of weight and the position of the site, such that the areas

of the cells meet the requirement. The final layout requires that the area of each cell should be in proportion to the associated value. In practice, if the area error is smaller than a threshold, then we will say the requirement is met and the iterative process is converged. Formally, let $value_{s_i}$ be the associated value of site s_i and $E_{threshold}$ be the threshold of the area error, then the convergent requirement can be expressed as:

$$\frac{\sum_{s_i \in S} \left| A(v(s_i)) - A(\Omega) * \frac{value_{s_i}}{values} \right|}{A(\Omega)} < E_{threshold}. \quad (5)$$

Once the iterative process is converged, the above-mentioned processes recurse to subdivide child region until all the leaves of the hierarchy are represented by cells with desired areas.

4 Orthogonal Voronoi Treemap

In this section, we introduce our orthogonal Voronoi treemap algorithm (OVT). We first provide an overview of our algorithm in Sect. 4.1, and then we discuss the three main steps of our algorithm: initialize site status (Sect. 4.2), update site status (Sect. 4.3), and compute the weighted orthogonal Voronoi diagram (Sect. 4.4). Finally, we give some implementation details in Sect. 4.5.

The overall structure of our algorithm follows that of Nocaj and Branches [28]. Meanwhile, ours is different in the following aspects:

- a new initialization strategy;
- a modified site update strategy;
- a novel distance function;
- a heuristic algorithm for diagram generation;

4.1 Overview

In this paper, the proposed orthogonal Voronoi treemap follows the same rules as the traditional Voronoi treemap. Because of the recursive feature of treemaps, considering a single layer is sufficiently enough. A pseudo-code to compute single layer orthogonal Voronoi treemap is summarized in Algorithm 1.

Algorithm 1 : Compute Orthogonal Voronoi Treemap (single layer)

Input: $S; \Omega; W; i_{max}; E_{threshold}$;

Output: $v(S)$;

ComputeOVTreemap(S, Ω, W)

```

1: Initialization( $S, \Omega, W$ ) ;
2: error =  $+\infty$  ;
3:  $v(S) = \text{ComputeWOVDiagram}(S, \Omega, W)$  ;
4: for  $i = 1 : i_{max}$ 
5:    $[S, W] = \text{AdaptPositionsWeights}(S, v(S), W)$  ;
6:    $v(S) = \text{ComputeWOVDiagram}(S, \Omega, W)$  ;
7:    $error = \frac{\sum_{s_i \in S} \left| A(v(s_i)) - A(\Omega) * \frac{value_{s_i}}{values} \right|}{A(\Omega)}$  ;
8:   if  $error < E_{threshold}$ , then
9:     return  $v(S)$  ;
10:  end
11: end
12: return  $v(S)$  ;
```

An initialization process is first conducted on the hierarchical data to generate the initial positions and weight for each site. This is achieved by the function *Initialization*(S, Ω, W) (Line 1). Then, an initial weighted centroidal orthogonal Voronoi diagram by the function *ComputeWOVDiagram*(S, Ω, W) is generated based on the initial status of sites (Line 3). After that, an iterative process is taken to update the site status by the function *AdaptPositionsWeights*($S, v(S), W$) and redraw the diagram until meeting the converge requirement. To handle hierarchical data with multiple layers, then the function *ComputeOVTreemap*(S, Ω, W) will be called recursively.

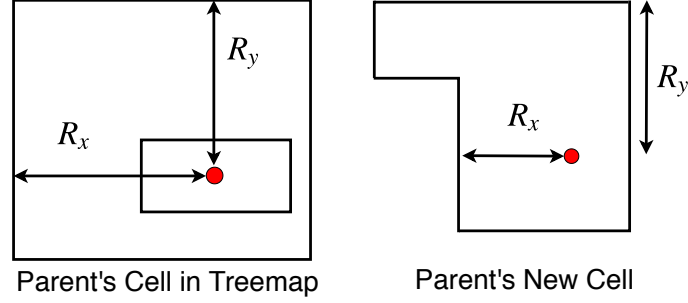


Figure 2: Transform the position of a site in rectangle cell of the treemap into the orthogonal rectangle cell as the initial position.

4.2 Initialization

The initialization step refers to the determination of the initial position of each site and the initial value of weight which is used to control the area of cell. Instead of a random initial value, a reasonable initial site status can significantly improve the algorithm performance. In this section, we determine the layout initial status including the initial status and the initial weight with the help of the treemap layout.

To start with, the hierarchical dataset is visualized by the squarified treemap algorithm [14] since it has been proved that the squarified treemap has a good aspect ratio [33]. It should be noted other treemap algorithm also can be used here. Once the treemap is plotted, we generate a site at the center of each rectangle and calculate the relative position of this site respect to its parent’s rectangle boundary. As shown in Fig. 2 (left), the value of R_x and R_y is then rescaled to the interval $[0, 1]$, respecting to the size of the outer rectangle. This relative position is set as the initial position of this site. When it is used in our algorithm, this relative position of that site is decoded according to its parent’s new cell. This decoding is conducted by considering R_y first and then R_x . In this way, the position of sites in the treemap will be transformed into the orthogonal rectangles of our plot as the initial position. For the initial weight value, we set it to the half of the area of the site’s cell in the treemap. Our experiments show that with these initial setting the final layout is much better than that with random initial status.

4.3 Site Status Update

To update the weight value and the position of each site, we make modification on the strategy used by Hahn et al. [29] since our orthogonal segmentation is different. Instead of updating position and weight separately, we merge these two functionalities into one and make modifications based on our case. The pseudo code for the function $AdaptPositionsWeights(S, v(S), W)$ is depicted in Algorithm 2. The main difference between our new $AdaptPositionsWeights(S, v(S), W)$ and previous methods [28, 29] is that we do not need to check the maximum weight value allowed for each site during the adjustment. The reason is that when we generate the segmentation lines, we have taken the overweight case into consideration (Sect. 4.4.1) in order to avoid the generation of empty cells.

4.4 Computation of the Orthogonal Voronoi Diagram

In this section, we describe the computation of the proposed orthogonal Voronoi diagram. Since the diagram is formed by segmentation lines between sites, the strategy to partition the space between two sites is important. According to Eq. 1, the space partitioning can be treated as a clustering of points based on the sites, if the whole plane is covered by uniformly distributed points. There are two main problems arose here. The first problem is how to calculate the distance to the sites, while the second is that for a certain point which site should it belong to. These two problems are straightforward when using the Euclidean distance in the Voronoi diagram. However, they are tough when trying to axis-alignedly subdivide the bounded region. To achieve this, we introduce a new distance function in Sect. 4.4.1 as well as how to find the reference site among multiple sites in Sect. 4.4.2.

Once the partition between two sites is confirmed, how to allocate the partitioned spaces to form a diagram is considered. Here, a sweepline + skyline heuristic algorithm is introduced in Sect. 4.4.3.

Algorithm 2 : Adapt positions and weights.

Input: S ; $v(S)$; W ;

Output: S ; W ;

AdaptPositionsWeights(S , $v(S)$, W)

```

1:  $f_s = 0$  ;
2: foreach  $s_i \in S$ 
3:    $c_i = \text{centroid}(v(s_i))$  ;
4:    $A_{\text{current}} = A(v(s_i))$  ;
5:    $A_{\text{target}} = A(\Omega) * \frac{\text{value}_{s_i}}{\text{value}_S}$  ;
6:    $f_{\text{adapt}} = \frac{A_{\text{target}}}{A_{\text{current}}}$  ;
7:   if  $f_s \neq 0$  and  $\text{sgn}(f_{\text{adapt}} - 1) \neq \text{sgn}(f_s - 1)$ , then
8:      $f_{\text{adapt}} = \min(1 + \rho, \max(f_{\text{adapt}}, 1 - \rho))$  ;
9:   end
10:   $w_i = \max(w_i * \sqrt{f_{\text{adapt}}}, \epsilon)$  ;
11:   $f_s = f_{\text{adapt}}$  ;
12:   $s_i^* = s_i + (c_i - s_i) * (1 - 0.5\rho)$  ;
13:  if  $s_i^*$  within  $v(s_i)$ , then
14:     $s_i = s_i^*$  ;
15:  else
16:     $s_i = s_i$  ;
17:  end
18: end
19: return  $S$ ,  $W$ ;

```

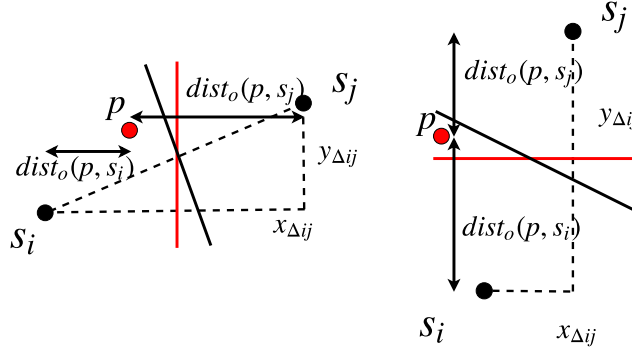


Figure 3: Two kinds of relative positions for sites s_i and s_j where $x_{\Delta ij} = |x_i - x_j|$ and $y_{\Delta ij} = |y_i - y_j|$. The black solid line is the segmentation based on Euclidean distance while the red solid line is an axis-aligned segmentation. The distance $\text{dist}_o(p, s_i)$ and $\text{dist}_o(p, s_j)$ in both cases are illustrated.

4.4.1 Distance Function

The new distance function considers the relative positions of two sites rather than only one site in previous distance function. Formally, when calculating the distance of point p and site s_i , we consider the relative positions of site pair s_i and s_j to decide which coordinate should be considered. Since we try to divide the space axis-aligned, we consider two kinds of relative positions between site s_i and s_j based on their x-axis difference $x_{\Delta ij} = |x_i - x_j|$ and y-axis difference $y_{\Delta ij} = |y_i - y_j|$. Then for an arbitrary point p , the distance to site s_i in both cases are depicted in Fig. 3 and defined as:

$$\text{dist}_o(p, s_i) = \begin{cases} |x_p - x_{s_i}| & \text{if } x_{\Delta ij} > y_{\Delta ij}, \\ |y_p - y_{s_i}| & \text{if } x_{\Delta ij} < y_{\Delta ij}. \end{cases} \quad (6)$$

When a positive weight value is associated with each site, the distance function (Eq. 6) should be modified as:

$$\text{dist}_o(p, s_i) = \begin{cases} |x_p - x_{s_i}| - w_i & \text{if } x_{\Delta ij} > y_{\Delta ij}, \\ |y_p - y_{s_i}| - w_i & \text{if } x_{\Delta ij} < y_{\Delta ij}. \end{cases} \quad (7)$$

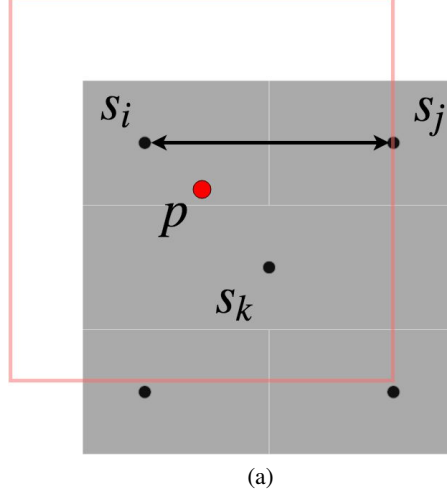


Figure 4: One example for choosing the reference sites for certain point p in red. A square in pink centered at the point p is built, including at least one horizontal site pair and one vertical site pair. By first considering horizontal site pair s_i and s_j , and then vertical site pair s_i and s_k , point p has smallest distance to site s_i .

For the left-hand-side case in Fig. 3, a vertical line is needed to separate the site pair while a horizontal line for the right-hand-side case in Fig. 3. Hence, the axis-aligned segmentation line L is defined as:

$$L_{s_i s_j} : \begin{cases} x = \frac{1}{2}(x_{s_i} + x_{s_j}) & \text{if } x_{\Delta ij} > y_{\Delta ij}, \\ y = \frac{1}{2}(y_{s_i} + y_{s_j}) & \text{if } x_{\Delta ij} < y_{\Delta ij}. \end{cases} \quad (8)$$

If two sites have large $y_{\Delta ij}$, then they will be separated by a horizontal line. Otherwise, these two sites will be separated by a vertical line. For the case that $x_{\Delta ij} = y_{\Delta ij}$, we break the tie by choosing a horizontal segmentation.

To guarantee that there is no cell with empty region, the segmentation lines should be located in between. This is based on an assumption that the sum of w_i and w_j are smaller than the distance between two sites. However, it is possible that this assumption fails. In this case, we partition the space according to the ratio of the weight values by the function $GenerateWLine(s_i, s_j, w_i, w_j)$. A pseudo-code for this function is depicted in Algorithm 3.

Algorithm 3 : Generate Weighted Segmentation Line

Input: $s_i; s_j; w_i; w_j;$

Output: $L_{s_i s_j};$

$GenerateWLine(s_i, s_j, w_i, w_j)$

- 1: **if** site s_i and s_j are horizontal neighbors, **then**
 - 2: **if** $|x_{s_i} - x_{s_j}| - w_i - w_j \geq 0$, **then** $L_{s_i s_j} = \min(x_{s_i} + w_i, x_{s_j} + w_j) + \frac{1}{2}(|x_{s_i} - x_{s_j}| - w_i - w_j);$
 - 3: **else** $L_{s_i s_j} = (x_{s_i} < x_{s_j}) ? x_{s_i} + \frac{w_i}{w_i + w_j} * |x_{s_i} - x_{s_j}| : x_{s_j} + \frac{w_j}{w_i + w_j} * |x_{s_i} - x_{s_j}|;$
 - 4: **end**
 - 5: **else**
 - 6: **if** $|y_{s_i} - y_{s_j}| - w_i - w_j \geq 0$, **then** $L_{s_i s_j} = \min(y_{s_i} + w_i, y_{s_j} + w_j) + \frac{1}{2}(|y_{s_i} - y_{s_j}| - w_i - w_j);$
 - 7: **else** $L_{s_i s_j} = (y_{s_i} < y_{s_j}) ? y_{s_i} + \frac{w_i}{w_i + w_j} * |y_{s_i} - y_{s_j}| : y_{s_j} + \frac{w_j}{w_i + w_j} * |y_{s_i} - y_{s_j}|;$
 - 8: **end**
 - 9: **end**
 - 10: **return** $L_{s_i s_j};$
-

4.4.2 Clustering

Once the distance function is confirmed, the second question is that for point p , which site should it belong to after calculating the distance. According to Eq. 7, point p may have multiple distance value to the same site when considering different site pairs. To eliminate the confusion, we first define the concept of valid neighborhood relationship between sites. Then we describe a principle to handle the case with multiple site pairs from the perspective of point p .

For a site pair, if there are no other sites located in the rectangle region formed by the two sites, then these two sites are valid neighbors. In terms of the relative positions, these two sites are either horizontal neighbors (i.e. neighbors in the horizontal direction) or vertical neighbors (i.e. neighbors in the vertical direction). The valid neighbor sites can also be considered from the perspective of the final diagram. If the existence of site s_j contributes to the generation of the cell of site s_i , then site s_i and s_j are valid neighbors.

For the case when there are multiple sites around, we define a principle to do clustering. For easy understanding, we take the case in Fig. 4 as an example. Firstly, we design the smallest square (in pink) centered at point p , including multiple sites such that there are at least one pair of vertical valid neighbor sites (s_i and s_k) and one pair of horizontal valid neighbor sites (s_i and s_j). Secondly, the segmentation line between the horizontal neighbor sites determines which site the point p should belong to. Thirdly, suppose point p belongs to site s_i now, then check the distance between point p and all of the vertical neighbors of site s_i to find the smallest one. If site s_i has the smallest or second smallest vertical distance to point p , then point p will be clustered accordingly. Otherwise, extend the square until such a kind of case meets.

However, this principle is complex and not automatic. Hence, a computer-based algorithm should be designed to automatically execute this principle. In the next section, a sweepline + skyline algorithm is described to carry out the partitioning based on the new distance function.

4.4.3 Sweepline + skyline algorithm

The proposed sweepline + skyline algorithm aims to automatically partition the canvas into orthogonal sub-regions based on the new distance function proposed in Sect. 4.4.1. Our idea is motivated by the sweep line algorithm for Voronoi diagram [10] and the skyline strategy used in cutting and packing problem [11]. The sweep line used in our algorithm is a vertical line moving from left to right. When the sweep line hits a new site, the relationship of this new site and all its left-hand-side site pairs are checked to generate vertical or horizontal segmentation lines. Meanwhile, a skyline is defined to record the current segmentation lines for all active sites. When the sweep line hits a new site and new segmentation lines are generated, the skyline will be updated correspondingly.

Figure 5 illustrates an example for this process. As shown in Fig. 5 (a), for a given rectangular canvas with $width = 1000$ and $height = 680$, six sites are positioned based on their coordinates (we follow the image coordinate system where the y-axis is down). The size of the canvas and the positions of sites are the input value of our algorithm. The first step (Fig. 5 (b)) is to create a vertical sweepline and a vertical skyline. The sweepline is initially located on the left-most site s_A while the skyline is on the left-hand-side of the canvas. The length of both lines equal to the height of the canvas. The second step (Fig. 5 (c)) is to sweep the sweepline from left to right to hit the next site s_B . Since $y_{\Delta AB} = 272$ is larger than $x_{\Delta AB} = 96$, a horizontal line $L_{AB} : y = 296$ is built between site s_A and s_B . The skyline is then updated by adding a horizontal line segment. After checking all the left-hand-side site pairs of site s_B , the sweepline moves to the next site s_C (Fig. 5 (d)). Since site s_A is not closed and is the horizontal neighbor of site s_C , then a vertical line $L_{AC} : x = 208$ is built. Once a vertical line is generated, the left site s_A of this horizontal neighbor sites should be closed and the bounding polygon of site s_A is formed based on the current skyline and the new vertical segment (as well as the canvas boundary). After that, the skyline is updated. Since site s_B is not closed and is the vertical neighbor of site s_C , then a horizontal line $L_{BC} : y = 256$ is built and the skyline is updated again (Fig. 5 (e)). This process is repeated until the sweepline reaches the last site s_F (Fig. 5 (f)). The residual sites (s_E and s_F) will then be closed and the bounding polygon for each site is formed by the current skyline and sweepline together. A pseudo-code for the whole process is depicted in Algorithm 4.

4.5 Implementation

The implementation of our proposed algorithms is in JavaScript. Our code mainly depends on the D3.js package [34] and previous implementation on the Voronoi treemap [35]¹. The color schema for some of the plots in this paper is generated by the Tree Color [12], such as Fig. 1 (b, c). The source code of our implementation can be found in Github.

Algorithm 4 : Compute Orthogonal Voronoi Diagram**Input:** $S; \Omega; W;$ **Output:** $v(S);$ *ComputeWOVDiagram* (S, Ω, W)

```

1: Sort  $S$  in the order of  $x_{s_i}$  ascending ;
2: Initialize  $L_{sweepline}$  ;
3: Initialize  $L_{skyline}$  ;
4: Initialize  $v(S) = []$  ;
5: for  $i = 1 : n$ 
6:   for  $j = 1 : i - 1$ 
7:     if site  $s_j$  is closed, then
8:       continue;
9:     end
10:    if site  $s_j$  is not the valid neighbor of site  $s_i$ , then
11:      continue;
12:    end
13:    if site  $s_i$  and  $s_j$  are vertical neighbors, then
14:       $L_{s_i s_j} = \text{GenerateLine}(s_i, s_j, w_i, w_j)$  ;
15:      Update  $L_{skyline}$  with  $L_{s_i s_j}$ ;
16:    else
17:       $L_{s_i s_j} = \text{GenerateLine}(s_i, s_j, w_i, w_j)$  ;
18:      Mark site  $s_j$  as closed;
19:      Generate the bounding polygon  $v(s_j)$  for site  $s_j$ ;
20:       $v(S).push(v(s_j))$ ;
21:      Update  $L_{skyline}$  with  $L_{s_i s_j}$ ;
22:    end
23:  end
24:  Update  $L_{sweepline}$ ;
25: end
26: for  $i = 1 : n$ 
27:   if site  $s_i$  is closed, then continue;
28:   else
29:     Generate the bounding polygon  $v(s_i)$  for site  $s_i$ ;
30:      $v(S).push(v(s_i))$ ;
31:   end
32: end
33: return  $v(S)$ ;

```

Table 1: The running time (in *ms*) for a single iteration.

| | 50 | 100 | 150 | 200 | 250 | 300 | 350 | 400 | 450 | 500 | 550 | 600 |
|---------|------|------|------|-------|-------|-------|-------|-------|-------|-------|-------|-------|
| VT [28] | 0.22 | 0.3 | 0.43 | 0.61 | 0.79 | 1.05 | 1.19 | 1.43 | 1.82 | 1.94 | 2.2 | 2.52 |
| VT | 1.38 | 3.96 | 6.83 | 10.95 | 16.59 | 25.13 | 30.17 | 39.48 | 46.30 | 64.45 | 82.17 | 91.34 |
| OVT | 0.93 | 2.74 | 5.61 | 9.24 | 14.19 | 19.60 | 26.31 | 31.10 | 38.61 | 45.94 | 53.90 | 71.13 |

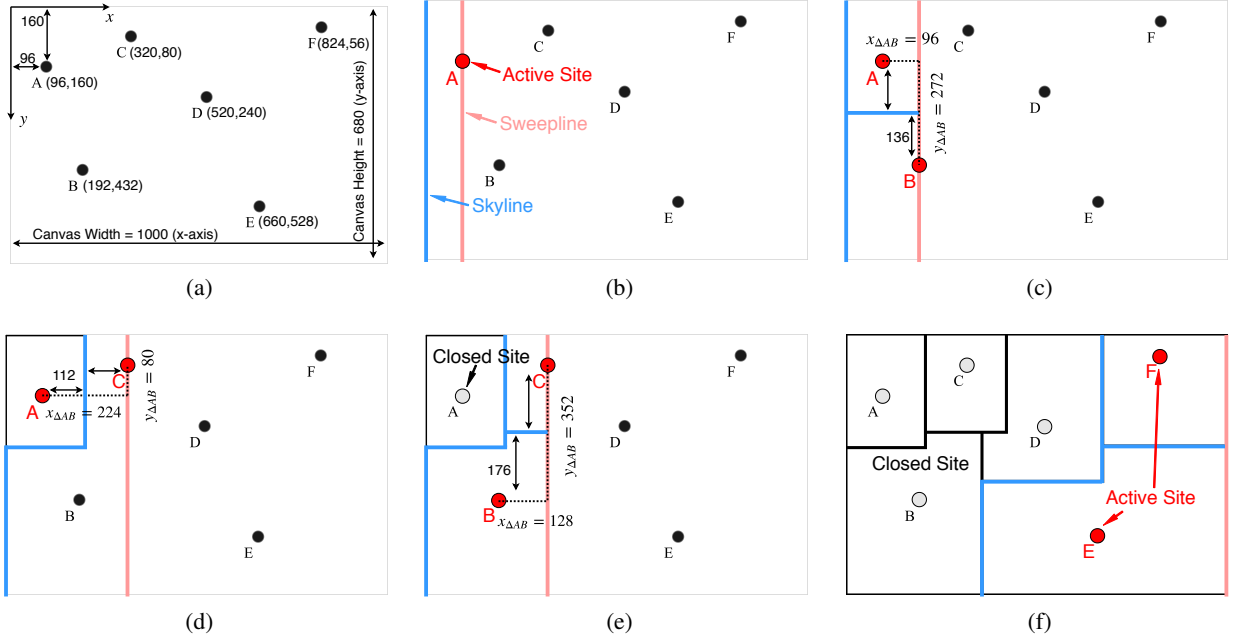


Figure 5: Overview of the sweepline + skyline algorithm. (a) Initially, six sites are positioned inside the canvas based on their initial positions. (b) The skyline (in blue) and the sweepline (in pink) are initialized and the first site s_A (left-most) is activated. (c) Sweep the sweepline to meet the second site s_B and determine the relationship of s_A and s_B . Then a horizontal segmentation line L_{AB} is added to the skyline. (d) Sweep the sweepline to site s_C and determine the relationship of s_A and s_C . Since s_A and s_C are horizontal neighbors, a vertical segmentation line is generated. In this case, site s_A is closed. A bounding polygon formed by the skyline and the canvas boundary and the vertical segmentation line is built for s_A . Then the skyline is updated and site s_A is marked as closed status. (e) Site s_B and s_C are then discussed and a horizontal segmentation line is added to the skyline. (f) The process is continued until the last site s_F is considered. All the active sites will be closed and the corresponding bounding polygon will be built based on the current skyline and the canvas boundary.

5 Performance

In the following, we evaluate the performance of our proposed algorithm from multiple aspects. First, we check the average number of site pairs and valid neighbors for each site since they have a strong relationship with the algorithm complexity in Sect. 5.1. Second, we compare our algorithm with the Voronoi treemap in terms of running time during a single iteration in Sect. 5.2. Then, the converging rate and the aspect ratio are analyzed in Sect. 5.3 and Sect. 5.4, respectively.

5.1 Site Pairs and Valid Neighbor

The number of neighbors for each site contributes to the computation complexity of our proposed algorithms. As depicted in Algorithm 4, all the non-closed sites will be checked to update the status by generating new segmentation lines and updating the skyline. This will lead to an $O(n^2)$ computation complexity. However, in practice, much fewer times are needed for the diagram to update its status. To show this, we generate a series of random datasets with a different number of sites (from 500 to 50000). For each dataset, the positions of sites are initialized randomly in an empty square canvas (900×900). We run our proposed algorithm on each dataset ten times to have a fair result since our tests are based on random data. During the experiments, two variables are recorded: the total number of site pairs checked and the total number of valid neighbors which change the diagram status. In the end, the average number of site pairs and the average number of valid neighbors per site are illustrated in Fig. 6 as box plots (noted that the x-axis is not linear).

¹ This JavaScript implementation is based on the work by Noca and Brandes [28] in which the program is run in Java.

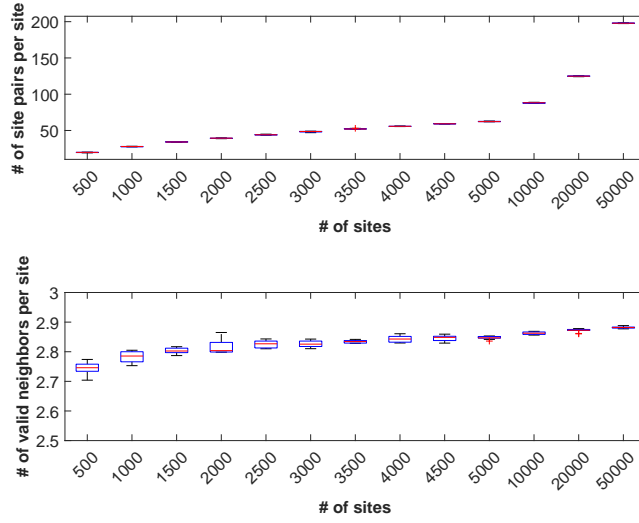


Figure 6: The average number of site pairs (top) and valid neighbors (bottom) per site. Noted that the x-axis is not linear.

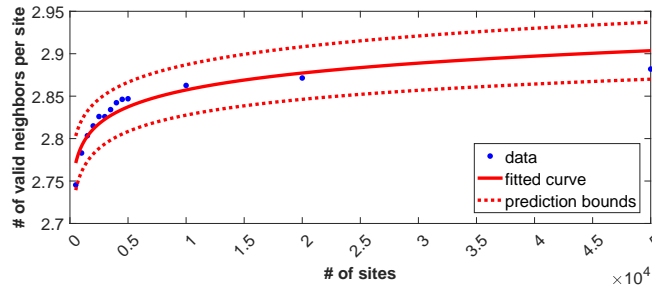


Figure 7: The fitting line and the prediction for the average number of valid neighbors per site.

The average number of site pairs per site refers to how many pairs of sites need to be checked for each site. If they are not valid neighbors, then the diagram status will not be changed. Since the check process is much less time expensive than updating the diagram, a small amount of computation time will be taken. It should be noted that the average number of site pairs per site is not linearly increased along the number of sites. We formulate the relationship between the number of sites and the average number of site pairs per site as follows:

$$\# \text{ of sitepairs per site} = 0.8563 * 2^{0.7256 * \log(\# \text{ of sites})} + 0.2494. \quad (9)$$

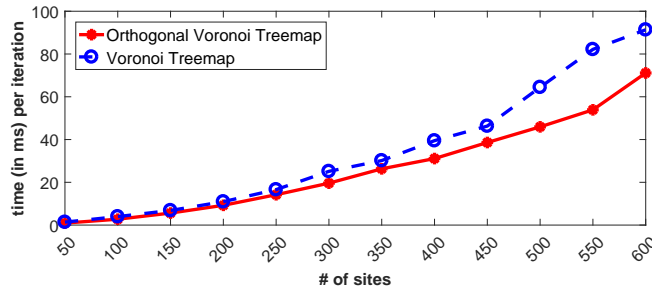
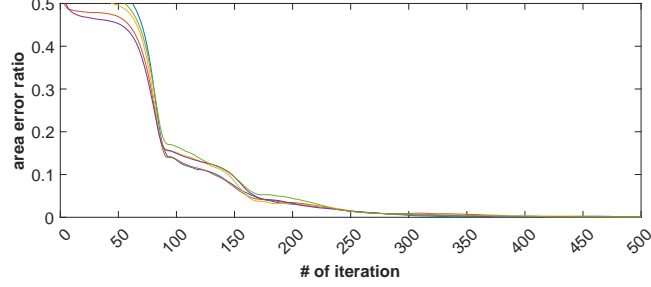
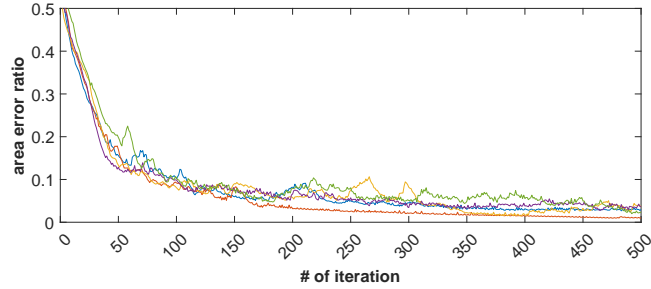


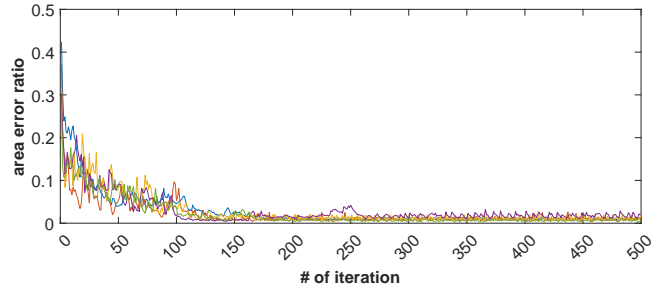
Figure 8: The running time (in ms) for a single iteration.



(a) Voronoi Treemap



(b) Orthogonal Voronoi Treemap with random initial status



(c) Orthogonal Voronoi Treemap with designed initial status

Figure 9: The converge rate of the Voronoi treemap, our orthogonal Voronoi treemap with random initial status and with our designed initial status. Within the 500 iterations, we record the area error of each iteration to indicate the converge rate.

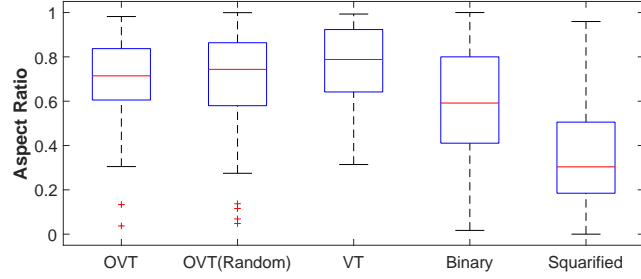
To evaluate the goodness of fit, we calculate the goodness-of-fit statistics including the sum of squares due to error (SSE), R-square, Adjusted R-square, root mean squared error (RMSE) [36]. In this case, the mean values in the boxplot are used for fitting and we get a good fitting with SSE=0.0664, R-square=1.0, Adjusted R-square=1.0, and RMSE=0.0815.

Although the number of site pairs per site is large, there are only limited valid neighbors which will lead to the change of the diagram status. According to Fig. 6 (bottom), we formulate the relationship by fitting, which can be expressed as:

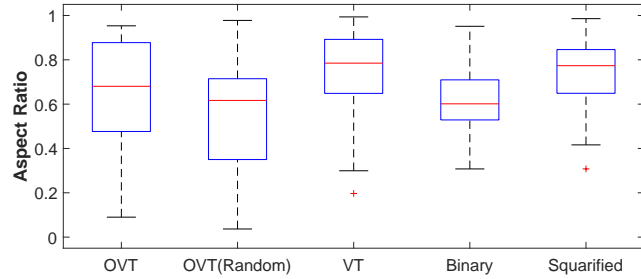
$$\# \text{ of valid neighbors per site} = 0.02875 * \log(\# \text{ of sites}) + 2.592. \quad (10)$$

The goodness-of-fit statistics in this case is SSE=0.0018, R-square=0.8929, Adjusted R-square=0.8832, and RMSE=0.0127 which indicate that the fitting function is suitable. We plot the fit and the prediction in Fig. 7.

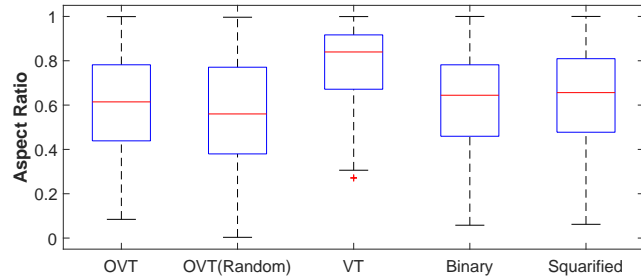
Formally, we can conclude that the computation complexity for a single iteration is $O(n \cdot \log(n))$ and the overall complexity is $O(k \cdot n \cdot \log(n))$ in Algorithm 4. Since the complexity for updating sites status (Algorithm 2) is linear, then we can show that the proposed orthogonal Voronoi treemap has $O(k \cdot n \cdot \log(n))$ complexity for a single layer hierarchical data.



(a) Test on random dataset



(b) Test on the globalGDP dataset



(c) Test on the Flare dataset

Figure 10: The boxplots of aspect ratio. In these tests, our orthogonal Voronoi treemap (OVT) has a comparable mean aspect ratio with the treemaps (binary treemap and squarified treemap). While the Voronoi treemap has the best aspect ratio in all tests.

5.2 Single Iteration Comparison

In addition to the computation complexity analysis above, we directly compare the running time of our algorithm during a single iteration to that of the Voronoi treemap. Although several running time are provided in the literature [5, 26, 28], we compare our algorithm with the approach of Nocaj and Brandes [28] since it is the fastest to date. However, their algorithm is implemented in a different programming language. To have a fair comparison, we utilize the JavaScript implementation of their algorithm instead. We run the JavaScript Voronoi treemap package [35] and our algorithm on the same computer (PC, Window 10, Intel Xeon CPU, 3.6 GHz, 16 GB memory). The experiment is also conducted on a series of random datasets with a different number of sites (from 50 to 600) which are associated with random values (approximately 30 % of sites with random values in $[0, 10]$ while the rest sites with random values in $[0, 1]$). For each dataset, both algorithms run 1000 iterations (we comment out the converge constraint in Algorithm 1 such that the algorithm will keep running until the maximum iteration number is reached). The average running time (in *ms*) is recorded in Table 1 and plotted in Fig. 8. Meanwhile, we list the concrete running time by Nocaj and Brandes [28] in Java as a reference.

Our algorithm needs less time per iteration than the Voronoi treemap as shown in Fig. 8 when both are run in the same programming language. The reason for this is that we modified the update sites status process in Sect. 4.3. In one

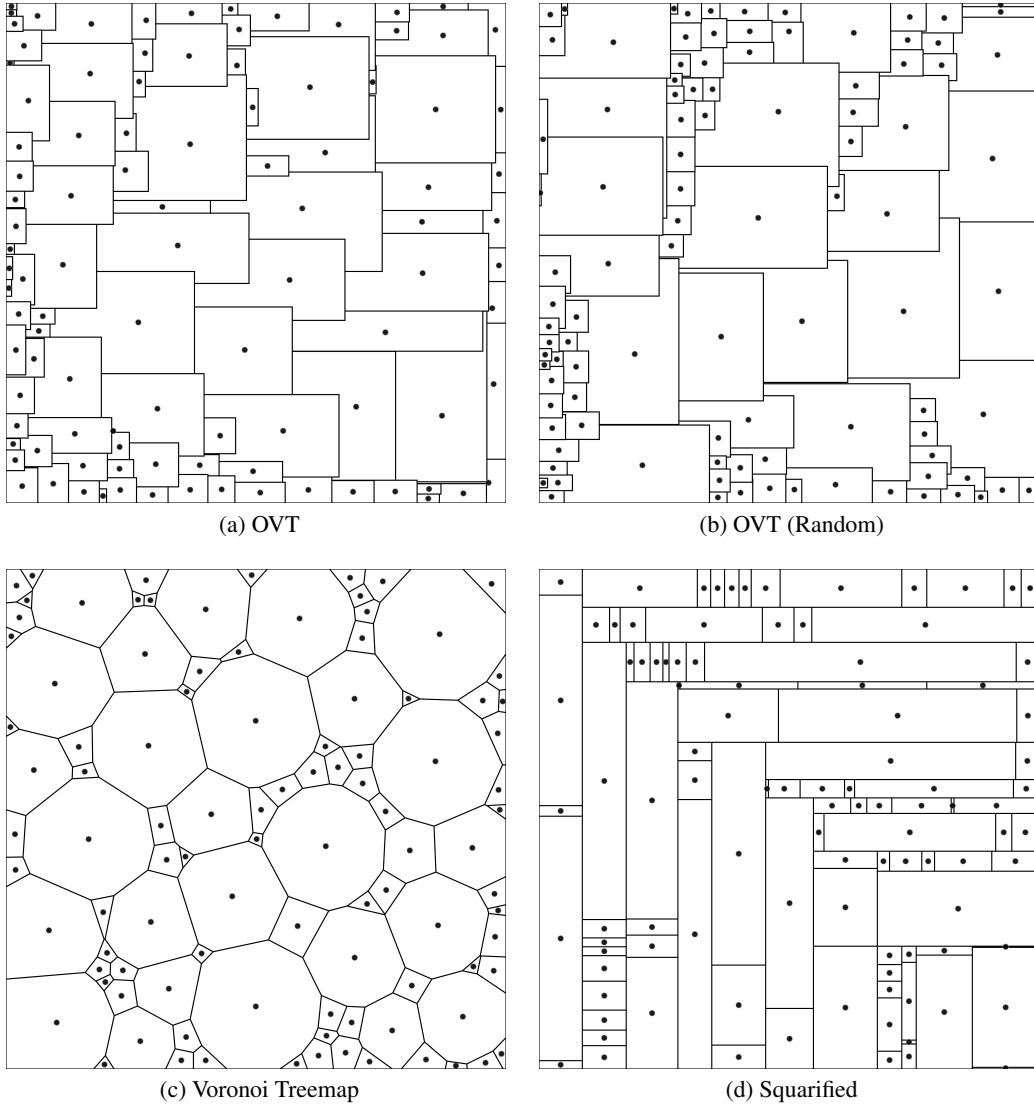


Figure 11: The final layouts on the random dataset.

iteration of the Voronoi treemap, it updates the sites' positions and weights, draws a Voronoi treemap, updates weights and then again draws a Voronoi treemap. In our modification, we merge the update of positions and weights into one step and handle the overweight case in the generation of segmentation line (Algorithm 3). Hence in one iteration of our algorithm, we only need to draw the orthogonal Voronoi treemap once rather than twice in the Voronoi treemap.

Compared with the original running time provided by Nocaj and Brandes [28], both our algorithm and the Voronoi treemap JavaScript package [35] need much more time. Since no hardware-accelerated code used in all cases, we believe that this difference is due to the capabilities of different programming languages. It would be one interesting future work to increase the efficiency by implementing the algorithm in Java in the backend and then displaying the results in JavaScript in the frontend.

5.3 Converge Rate

In this section, we test the converging speed of algorithms by considering the changes of the area error ratio along the iteration number increases, since the area of each element in the plot should match its associated value. Starting from initial positions and initial weights, the status of sites is updated iteratively as discussed in Sect. 4.3. To test the converging speed, we generate a single-layer hierarchical dataset with 200 random positioned sites which are associated

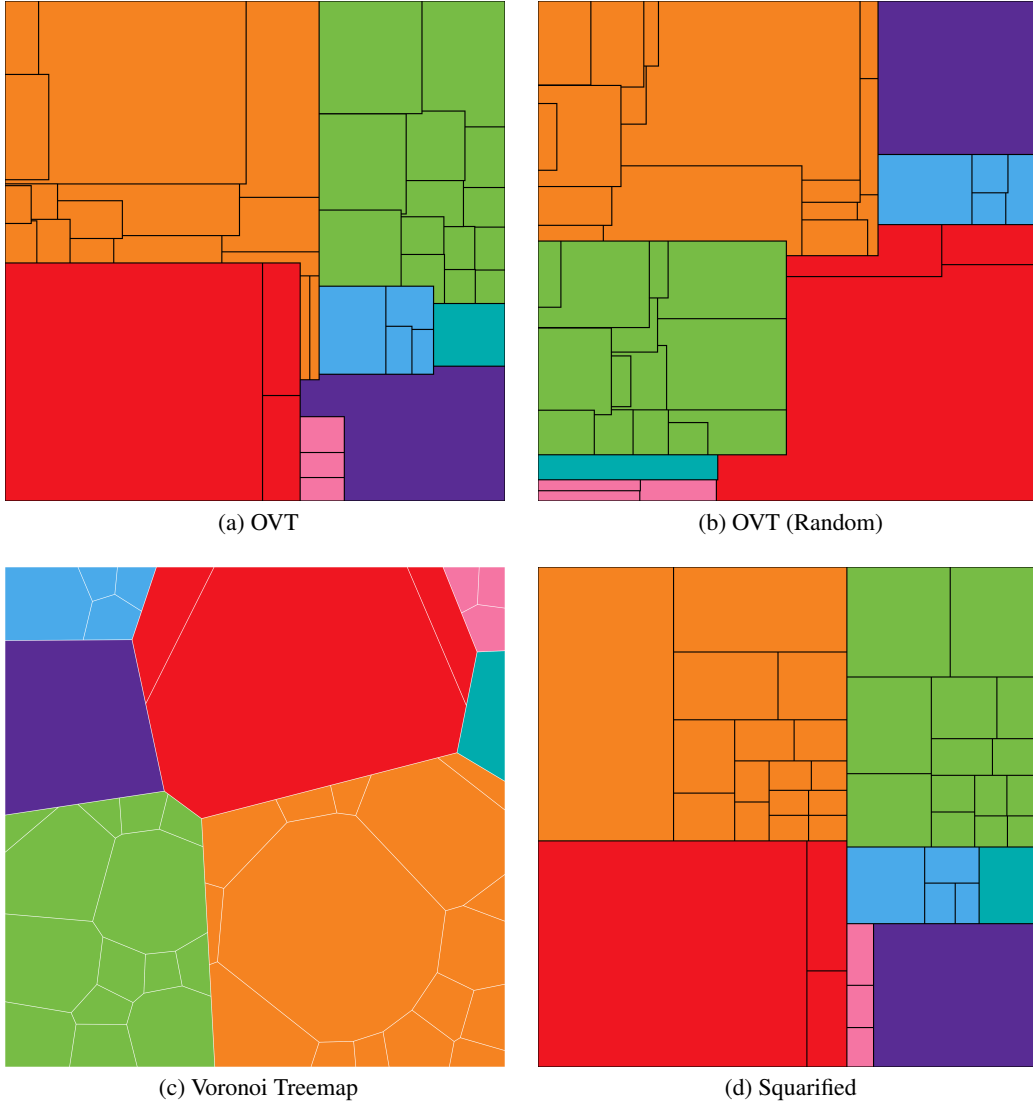


Figure 12: The final layouts on the globalGDP dataset.

with random values (approximately 30 % of sites with random values in $[0, 10]$ while the rest sites with random values in $[0, 1]$). Both the Voronoi treemap and our algorithms are run 5 times. Moreover, we compare our initialization strategy with a random initial status for our algorithms. We calculate and record the area error ratios of both algorithms in each iteration. The results are plotted in Fig. 9.

As illustrated, our algorithm with designed initial status performs better than that with random initial status and the Voronoi treemap. Compared with random initial status, the proposed initial status guarantees that the algorithm starts from a lower area error. Moreover, the area error ratio can reach a tough constraint (such as 0.01 area error ratio) within 200 iterations. While for our algorithm with random initial status, even after 500 iterations this tough constraint may not be satisfied. Compared with the Voronoi treemap with the random initial position and small positive weight, our algorithm generally converges faster. It is believed that the reason for this result is our reasonable initialization strategy. Since our orthogonal Voronoi treemap is similar to the treemap, using treemap to set initial status significantly contributes to the fast convergence in our algorithm. However, although our algorithm can converge under a tough constraint, it should be noted that our algorithm with both initial statuses has larger fluctuation than the Voronoi treemap. We consider that this is due to the non-consistent distance function used to partition the space (sometimes horizontal, sometimes vertical). While for the Voronoi treemap, the partitioning is straightforward.

5.4 Aspect Ratio

We discuss the aspect ratio of our algorithm and compare with the Voronoi treemap and different treemap layouts in this section. Our experiments are conducted on three datasets, including a random dataset (single layer with 100 sites), the global GDP dataset (two layers with 42 leaf nodes), and the Flare class hierarchy (four layers with 220 leaf nodes). For our algorithm and the Voronoi treemap, we set the maximum iteration number to 500 and the area error threshold for convergence to 0.01. For our algorithm and the treemaps, the aspect ratio of the axis-aligned minimum bounding box is calculated while for the Voronoi treemap, the aspect ratio of the oriented minimum bounding box is calculated. The result is illustrated as boxplots shown in Fig. 10. Meanwhile, we display the final layouts on the random dataset in Fig. 11 and the final layouts on the globalGDP dataset in Fig. 12. The final layout of our algorithm on the Flare data is shown in Fig. 1 (b,c) as well.

When considering the mean aspect ratio (the red line) in Fig. 10, our algorithm is better than treemap layouts on the random dataset and has similar results on two real datasets, although the Voronoi treemap has the best aspect ratio in three cases. When comparing the different initial status of our algorithm, we can find that with the designed initialization strategy our algorithm has a better aspect ratio (the closer to one the better) and small distribution range.

6 Discussion

Our algorithm has a comparable performance with the state-of-the-art Voronoi treemap algorithms in terms of computation complexity, computation time, converge speed, and aspect ratio. Moreover, according to the description of our algorithm, the proposed orthogonal Voronoi treemap is flexible to the changes of data value similar to the Voronoi treemap. Meanwhile, it utilizes nested orthogonal rectangles to present each cell and produces a rectangle-like layout.

There are also a few drawbacks in our algorithm. Firstly, as mentioned in Sect. 5.3, our algorithm has large fluctuation during the iteration. This shows that the area error in our algorithm is not monotonously decreasing. Fortunately, with our designed initialization strategy, the area error can be decreased to an acceptably small value. The second drawback is that the position of some sites in our algorithm may move in a large range. This leads to a non-stable layout. In the site status update procedure, we have no strategy used to preserve the relative positions of sites.

It would be an interesting future work for our algorithm to preserve the relative positions of sites during iteration in order to visualize dynamic hierarchical data for which a stable layout is essential [26, 29, 33]. Another future work is to utilize the treemap to visualize high-dimensional hierarchical dataset. Currently, the parameter associated to each site is usually only one dimension. When it comes to high-dimensional data visualization [37], how to visualize the values or other information while indicating the hierarchical structure would be an interesting direction.

7 Conclusion

In this paper, we described a novel algorithm for the Voronoi treemap with nested orthogonal rectangles. To the best of our knowledge, this is the first time the sweep line strategy is used to generate the Voronoi treemap. We proved that the proposed algorithm has an $O(n \cdot \log(n))$ complexity which is the same as the state-of-the-art Voronoi treemap. Moreover, by modifying the update procedure, it is proved that our algorithm requires less computation time than the Voronoi treemap in the same programming language. Owing to the designed initialization strategy, our algorithm converges faster than the Voronoi treemap and has comparable aspect ratio against the treemap. With a tidy layout by nested orthogonal rectangles and the adjustment capability by site status modification, the proposed orthogonal Voronoi treemap plays the role of the bridge in connecting the treemap and the Voronoi treemap.

References

- [1] Martin Graham and Jessie Kennedy. A survey of multiple tree visualisation. *Information Visualization*, 9(4):235–252, 2010.
- [2] Hans-Jorg Schulz. Treevis.net: A tree visualization reference. *IEEE Computer Graphics and Applications*, (6):11–15, 2011.
- [3] Hans-Jorg Schulz, Steffen Hadlak, and Heidrun Schumann. The design space of implicit hierarchy visualization: A survey. *IEEE Transactions on Visualization and Computer Graphics*, 17(4):393–411, 2011.
- [4] Ben Shneiderman. Tree visualization with tree-maps: 2-d space-filling approach. *ACM Transactions on Graphics*, 11(1):92–99, 1992.
- [5] Michael Balzer and Oliver Deussen. Voronoi treemaps. In *Proc. INFOVIS*, pages 49–56. IEEE, 2005.

- [6] Felipe SLG Duarte, Fabio Sikansi, Francisco M Fatore, Samuel G Fadel, and Fernando V Paulovich. Nmap: A novel neighborhood preservation space-filling algorithm. *IEEE Transactions on Visualization and Computer Graphics*, 20(12):2063–2071, 2014.
- [7] Michael Burch, Natalia Konevtsova, Julian Heinrich, Markus Hoferlin, and Daniel Weiskopf. Evaluation of traditional, orthogonal, and radial tree diagrams by an eye tracking study. *IEEE Transactions on Visualization and Computer Graphics*, 17(12):2440–2448, 2011.
- [8] Steve Kieffer, Tim Dwyer, Kim Marriott, and Michael Wybrow. Hola: Human-like orthogonal network layout. *IEEE Transactions on Visualization and Computer Graphics*, 22(1):349–358, 2016.
- [9] Mark de Berg, Bettina Speckmann, and Vincent van der Weele. Treemaps with bounded aspect ratio. *Computational Geometry*, 47(6):683–693, 2014.
- [10] Steven Fortune. A sweepline algorithm for voronoi diagrams. *Algorithmica*, 2(1-4):153, 1987.
- [11] E. K. Burke, G. Kendall, and G. Whitwell. A new placement heuristic for the orthogonal stock-cutting problem. *Operations Research*, 52(4):655–671, 2004.
- [12] Martijn Tennekes and Edwin de Jonge. Tree colors: color schemes for tree-structured data. *IEEE Transactions on Visualization and Computer Graphics*, 20(12):2072–2081, 2014.
- [13] Guanqun Wang, Tsuneo Nakanishi, and Akira Fukuda. 2-d layout for tree visualization: a survey. In *Proc. MATEC Web of Conferences*, volume 56. EDP Sciences, 2016.
- [14] Mark Bruls, Kees Huizing, and Jarke J Van Wijk. Squarified treemaps. In *Data Visualization 2000*, pages 33–42. Springer, 2000.
- [15] Ben Shneiderman and Martin Wattenberg. Ordered treemap layouts. In *Proc. INFOVIS*, pages 73–78. IEEE, 2001.
- [16] Benjamin B Bederson, Ben Shneiderman, and Martin Wattenberg. Ordered and quantum treemaps: Making effective use of 2d space to display hierarchies. *ACM Transactions on Graphics*, 21(4):833–854, 2002.
- [17] Ying Tu and Han-Wei Shen. Visualizing changes of hierarchical data using treemaps. *IEEE Transactions on Visualization and Computer Graphics*, 13(6):1286–1293, 2007.
- [18] Jo Wood and Jason Dykes. Spatially ordered treemaps. *IEEE Transactions on Visualization and Computer Graphics*, 14(6), 2008.
- [19] Yanchao Wang and Lujie Chen. Two-dimensional residual-space-maximized packing. *Expert Systems with Applications*, 42(7):3297–3305, 2015.
- [20] Takayuki Itoh, Yumi Yamaguchi, Yuko Ikehata, and Yasumasa Kajinaga. Hierarchical data visualization using a fast rectangle-packing algorithm. *IEEE Transactions on Visualization and Computer Graphics*, 10(3):302–313, 2004.
- [21] Aimi Kobayashi, Kazuo Misue, and Jiro Tanaka. Edge equalized treemaps. In *Proc. IV*, pages 7–12. IEEE, 2012.
- [22] Martin Wattenberg. A note on space-filling visualizations and space-filling curves. In *Proc. INFOVIS*, pages 181–186. IEEE, 2005.
- [23] Susanne Tak and Andy Cockburn. Enhanced spatial stability with hilbert and moore treemaps. *IEEE Transactions on Visualization and Computer Graphics*, 19(1):141–148, 2013.
- [24] Jie Liang, Quang Vinh Nguyen, Simeon Simoff, and Mao Lin Huang. Angular treemaps—a new technique for visualizing and emphasizing hierarchical structures. In *Proc. IV*, pages 74–80. IEEE, 2012.
- [25] David Auber, Charles Huet, Antoine Lambert, Benjamin Renoust, Arnaud Sallaberry, and Agnes Saulnier. Gospermap: Using a gosper curve for laying out hierarchical data. *IEEE Transactions on Visualization and Computer Graphics*, 19(11):1820–1832, 2013.
- [26] Avneesh Sud, Danyel Fisher, and Huai-Ping Lee. Fast dynamic voronoi treemaps. In *Proc. ISVD*, pages 85–94. IEEE, 2010.
- [27] David Gotz. Dynamic voronoi treemaps: A visualization technique for time-varying hierarchical data. *Phys. Rev. A*, 30(2):150–156, 2011.
- [28] Arlind Nocaj and Ulrik Brandes. Computing voronoi treemaps: Faster, simpler, and resolution-independent. In *Computer Graphics Forum*, volume 31, pages 855–864. Wiley Online Library, 2012.
- [29] Sebastian Hahn, Jonas Trümper, Dominik Moritz, and Jürgen Döllner. Visualization of varying hierarchies by stable layout of voronoi treemaps. In *Proc. IVAPP*, pages 50–58. IEEE, 2014.
- [30] Weixin Wang, Hui Wang, Guozhong Dai, and Hongan Wang. Visualization of large hierarchical data by circle packing. In *Proc. CHI*, pages 517–520. ACM, 2006.

- [31] Jochen Görtler, Christoph Schulz, Daniel Weiskopf, and Oliver Deussen. Bubble treemaps for uncertainty visualization. *IEEE Transactions on Visualization and Computer Graphics*, 24(1):719–728, 2018.
- [32] Qiang Du, Vance Faber, and Max Gunzburger. Centroidal voronoi tessellations: Applications and algorithms. *SIAM review*, 41(4):637–676, 1999.
- [33] Max Sondag, Bettina Speckmann, and Kevin Verbeek. Stable treemaps via local moves. *IEEE Transactions on Visualization and Computer Graphics*, 24(1):729–738, 2018.
- [34] D3.js. <https://d3js.org/>.
- [35] Voronoi treemap package in javascript. <https://github.com/Kcnarf>.
- [36] Mathworks: Evaluating goodness of fit. <https://ww2.mathworks.cn/help/curvefit/evaluating-goodness-of-fit.html>.
- [37] Yan Chao Wang, Qian Zhang, Feng Lin, Chi Keong Goh, and Hock Soon Seah. Polarviz: a discriminating visualization and visual analytics tool for high-dimensional data. *The Visual Computer*, pages 1–16, 2018.